DESIGN AND DEVELOPMENT OF A NOVEL COMPACT SOFT-SURFACE STRUCTURE FOR PERFORMANCE IMPROVEMENT AND SIZE REDUCTION OF A MICROSTRIP YAGI ARRAY ANTENNA

A Thesis Presented to the Academic Faculty

by

Trang Thuy Thai

In Partial Fulfillment of Institute Requirements
for the Degree of Bachelor of Science in Electrical Engineering
with Thesis Option

School of Electrical and Computer Engineering
Georgia Institute of Technology

May 2008

ACKNOWLEDGEMENTS

I would like to acknowledge the support of the Georgia Electronic Design Center, and would to thank Per O. Iversen, SATIMO USA for supplying the microwave chamber in the antenna radiation measurement. In addition, I am profoundly grateful to my advisors, Prof. Manos Tentzeris and Dr. Gerald DeJean, who have given me the guidance that has significantly influenced my academic career through the last two years of my undergraduate study at Georgia Tech. Without the advice and encouragement of Prof. Tentzeris and Dr. DeJean, this thesis would not be possible, nor would I have considered pursuing a graduate study. The mental and financial support of Prof. Tentzeris was tremendous and highly appreciated especially during the hard times that I've encounter in my undergraduate years as well as in my research experiences. The mentorship of Dr. DeJean was the most fortunate thing that I have received in my undergraduate research. Through patience and great knowledge, Dr. DeJean has motivated and helped me grow intellectually; thus along with Prof. Tentzeris' vision I was able to achieve many goals I once considered far from reach. I would also like to thank Prof. John Papapolymerou and Prof. Joy Laskar for letters of recommendation, Dr. Ronglin Li and Dr. Symeon Nikolaou for helping me with measurement set up, as well as all members of ATHENA Research group for making the research place an enjoyable and supporting environment. Finally, my life and the entire education are deeply owed to my parents, Thai Kien Dinh and Nguyen Thi Nga, who have made constant and incomparable sacrifices in order for my sister, my brother, and me to fly far and high. I am in endless debt to my beloved family.

I. INTRODUCTION

An antenna is a device (usually metallic) that is designed to transmit and receive electromagnetic waves and convert them into electrical signals and back to space waves. It is the transitional structure between free space and the guiding structure or transmission line (coaxial line, hollow pipe or other waveguide structures) that guides the converted electrical signals to and from other electrical units on an electronic application in a communication process. A typical communication system (receiver) is illustrated in Fig. 1a, it shows an antenna connected to a television through a coaxial line to receive signals. Figure 1b shows an equivalent circuit representation of the system in Fig. 1a where Vs is the voltage source and Zs, Zo, and ZL are the impedance representations of the source, the coaxial line and the antenna respectively. Other typical applications include radios, mobile phones, wireless router for internet, television base stations, radars.

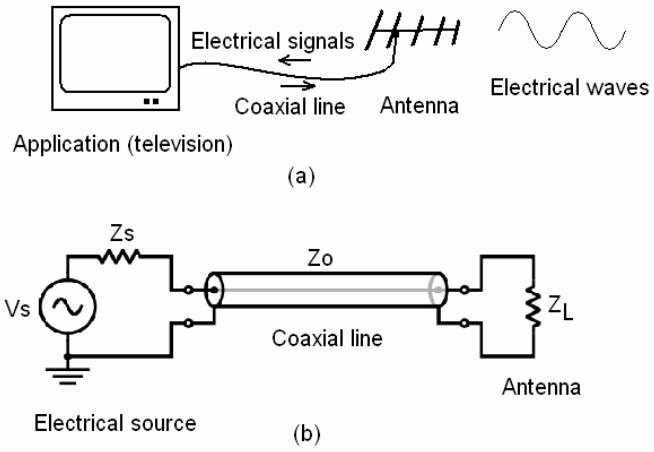

Figure 1. Illustration of a wireless device for a.) Schematic of physical connection between devices; and b.) Schematic of the corresponding electrical connection.

Pioneered by the work of Hertz and Tesla, the invention of wireless telegraph was developed from the 1880s, and since then the communications industry has become a

vital part of modern technology. Thus antennas and their principles have become the center focus because they enable the wireless transmissions by establishing the electrical links between devices wirelessly.

Antennas exist in many forms and types, and its variety continues to grow in the development of the wireless communication technology. The most common and simple type of antennas are dipole or monopole antennas which consist of common straight wires, and they have omni-directional radiation pattern. Other common types include loop antennas, pyramidal horns, conical horns, and rectangular waveguides. These are shown in Fig. 2. Other types of antennas include Yagi-Uda arrays, aperture arrays, helical antennas, log-periodic antennas, microstrip antennas, and slotted antennas. Among these, Yagi-Uda arrays or Yagi arrays and microstrip antennas have had important impacts in the development of wireless techonology. The original design of a Yagi-Uda array was first introduced by S. Uda in Japan in the early 1920s, described in English by H. Yagi and is now a classic and is fundamental to antenna development. The topology of the Yagi-Uda array (Yagi) consists of a number of elements. The element that is excited with a direct source of energy is called the driven element, and others are parasitic radiators with currents induced from the driven element (Fig. 3a). The concept of microstrip antennas was first introduced in the 1950s but did not receive considerable attention until the 1970s. Microstrip antennas consist of a printed metal conductor on top of a substrate and a ground plane underneath the substrate (Fig. 3b).

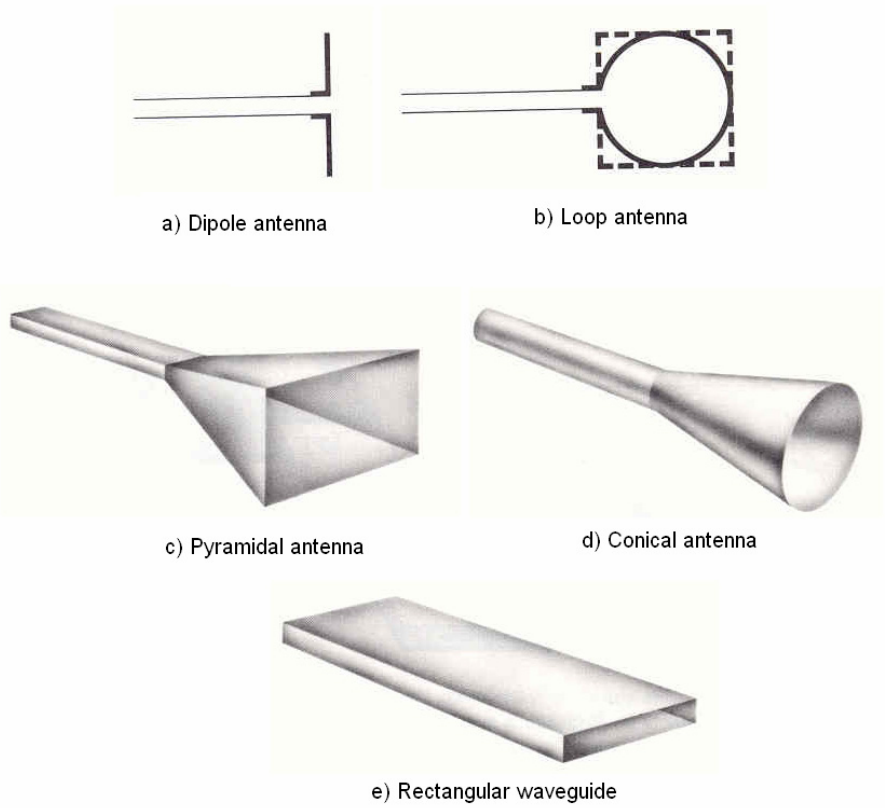

Figure 2. Common types of antennas (usually made with copper)[1].

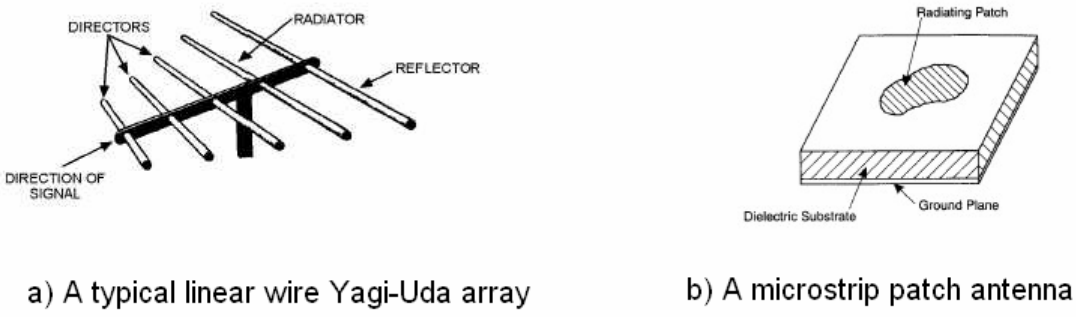

Figure 3. Typical forms of a.) a Yagi-Uda array; and b.) a microsstrip antenna.

The antenna performance is characterized by different parameters which typically include but are not limited to radiation pattern, directivity, gain, front-to-back ratios,

bandwidth, beam width, and radiation efficiency [1]. Among these, radiation pattern, directivity, and gain are crucial to a class of antennas known as the directional antennas. A directional antenna can transmit and receive signals significantly effectively in some directions more than in others. Its radiation pattern of the electromagnetic field is said to be directive.

Other considerations regarding the merits of the antennas include size, ability to integrate with circuit technologies such as monolithic microwave integrated circuits (MMICs), easy fabrication, and low cost. In this thesis document, a highly directional and compact antenna is designed and developed to improve the performance of a microstrip Yagi array antenna that was previously proposed. The design employs a high impedance surface structure called soft surface structure to enhance the radiation pattern of the planar microstrip antennas.

II. BACKGROUND

Due to the increasing demand for low profile, light weight, low cost, and easy integration into arrays and microwave integrated circuits, microstrip patch antennas have been one of the most innovative developments in antenna research in recent years [2][3][4] . Among various applications, directional antenna arrays are especially needed for most wireless local area network (WLAN) applications to suppress unwanted interference and to optimize power efficiency and coverage range. Since the Yagi-Uda antennas operate as endfire arrays [1], they are used in numerous industrial, scientific, and medical (ISM) applications at 2.4 GHz where directional radiation is necessary for long-distance wireless / point-to-point communications; high performance WiFi networks

at 5-6 GHz, and ultra-broadband millimeter-wave applications above 30 GHz (wireless multimedia, ad-hoc sensor networks) require high gain (> 10 dBi) and quasi-endfire radiation to alleviate propagation loss effects through line-of-sight reception of waves at angles off broadside.

However, Yagi arrays have disadvantages because they are bulky, thus being unsuitable for compact integration with microwave monolithic integrated circuits (MMICs) and RF circuitry due to their size [5], [6]. Various efforts attempting to combine the directional characteristics of the Yagi arrays with the advantages of microstrip antennas , such as printed Yagi antennas, have been proposed over the last 15 years [7]– [13]. The use of Yagi antenna designs in microstrip technology was first presented by Huang in 1989 in a four-patches configuration with a radiation peak between 30– 40° [7]. To achieve a gain as high as 14 dBi, Densmore and Huang introduced microstrip Yagi arrays consisting of four elements in four rows. The driven elements in each row are excited simultaneously [8], [9]. However the F/B ratios of around 4–5 dB may not be suitable for many applications. Different techniques have been proposed and utilized to improve the gain and F/B ratios of microstrip Yagi antennas. Techniques used include utilizing periodic bandgap (PBG) structures [10], and conventional soft-hard-surface (SHS) structures [14]. However, these structures require complicated and costly fabrication processes.

As a conclusion, there is a tradeoff for existing printed Yagi array antennas between achieving a high gain and maintaining a high F/B ratio as well as low cross-polarization and easy fabrication. One Yagi array that has been proposed for millimeter wave frequencies [13] radiates in the end-fire direction with a high gain of 11.7dBi, and

features a low cost, low profile, circular polarization and electrically steered beam, but its lateral size is big. In DeJean et al. [15], a new microstrip Yagi array design was proposed that could achieve a high gain (>10 dBi) and a F/B ratio of about 15 dB difference among the peaks between $0^o \leq \theta \leq 90^o$ and $-90^o \leq \theta \leq 0^o$, which is higher than previously published ratios. However, this F/B ratio has a low bandwidth (about 7%), that is not high enough for applications such as wireless multimedia/ HDTV.

A new configuration is proposed in this thesis document based on the antenna in DeJean et al. [15] implemented with a soft surface (SS) ring, that can improve the F/B ratio by at least 3 dB while maintaining high gain and low cross polarization as well as sustaining a high F/B ratios in a bigger bandwidth. In contrast to the conventional SHS, which is difficult to manufacture and requires a large area [16], the innovative SS structure introduced in Ruvio et al. [17] consists of quarter-wavelength metal strips that are short-circuited to the ground plane. This concept of the modern SS allows for its robust implementation and easy fabrication with standard double sided clad-boards. It was demonstrated to improve the radiation pattern of a simple patch antenna in Li et al. [18] and will be utilized in the planar array in this thesis. The SS structure consists of four metal strips connected together to form a ring; the metal strips are shorted to the ground through short metallized walls. Without loss of generality, their vertical length has been chosen to be equal to the substrate thickness, which is 0.046 λ_{eff} (62 mils). The F/B ratios here are defined in two pairs of quadrants of angle θ on the E-plane. "F/B-Left" is defined as the ratio between the radiation peak in the range of $0^o \leq \theta \leq 90^o$ (quadrant I) and that in the range of $-90^o \leq \theta \leq 0^o$ (quadrant II). "F/B-Right" ratio is defined as the ratio between the radiation peak in the range of $0^o \leq \theta \leq 90^o$ (quadrant I) and that in the range of

$90^o \leq \theta \leq 180^o$ (quadrant III). The proposed design architecture can produce significantly higher F/B ratios (more than 20 dB) and a size reduction by a factor of 1.5-2. The design also enables the development of multilayer (3D) ultra-wideband cognitive RF modules that could be deployed in automotive collision-avoidance radars and in numerous compact portable and sensing devices.

III. IMPLEMENTATION OF THE SS STRUCTURE

The concept of SHS was first considered by Kildal in [19]. When a plane wave is incident on a plane surface reflector with corrugations straight and transverse to the direction of the incident wave, the surface can be conditioned to be soft when the depth of the transverse corrugations is a quarter wavelength. Since then, there have been many developments on the SHS structures and a modern realization of artificial SS structure has been introduced in Ruvio et al.[17] and applied to a rectangular patch antenna in Li et al. [18]. In this thesis document, another implementation of this modern SS structure is presented.

Based on the original microstrip Yagi array antenna [15] (denoted as model A in Fig. 4a), and having the microstrip feed line replaced by the coaxial feed line (model B in Fig. 4b), the SS ring is built around the antenna structure on different ground sizes as shown in model C (Fig. 5) and model D (Fig. 6). In Model D, the ground plane is reduced to that of the outer edge of the SS ring in contrast to Model C. Figure 7 shows a 2D illustration of the dimensional variables of Model C (and in effect, Model D without the ground plane outside the SS ring). These two models are excited by a 50 Ω coaxial line fed through the substrate from underneath the antenna and have the same dimensions

from inside the outer edge of the SS ring. The design consists of a compact SS rectangular ring, S_i, made of metal strips that are shorted to the ground plane through metallized walls and S_W, which are placed along the outer edge of the metal strips. In fabrication the metal walls are realized by utilizing metal vias. All the metal strips have the same optimized width, denoted Q_S, which is $\lambda_g/4$ where λ_g is the guided wavelength $\lambda_g = \lambda_o/\varepsilon_{eff}$ ^0.5 (where ε_{eff} is the effective dielectric constant with a value between 1 and ε_r, and λ_o is the free space wavelength). The inner width of the SS ring, W_S, is approximately one λ_o. The inner length of the SS ring, L_S, is approximately 1.7 λ_o. These optimized parameters are explained in the next section. Additionally, these principles are justified in Section V where the parametric analysis of the SS ring is performed.

The optimized physical dimensions (in mils) for models B, C, and D are summarized in Table 1. While all the parameters are indicated in Fig. 7, the major dimensions are denoted as follows: the length and width of the driven element, "D", are L_D and W_D; the lengths and widths of director 1, "D1", and director 2, "D2", are L_{D1}, W_{D1}, L_{D2} and W_{D2}; the length and width of the reflector, "R", is L_R and W_R respectively. The ground length and width of model C is 5300 x 4000 mils (Fig. 5); the ground length and width of model D is 4135 x 2904 mils (Fig. 6). The dimensions of the driven element, "D", the directors D1 and D2, the reflector and their relative positions are chosen based on the constructive interference principles that were described in [15]. Without loss of generality, the structure was designed around the operating center frequency of 5.8 GHz for WiFi applications.

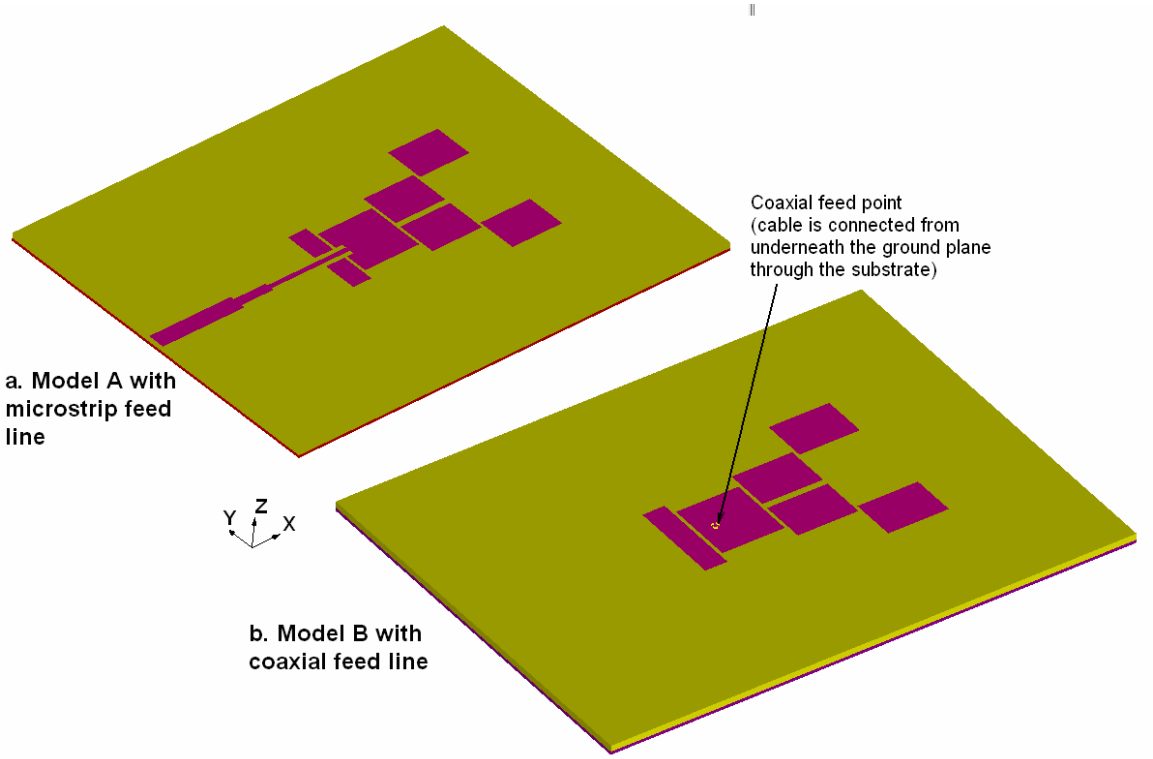

Figure 4. The topology of models without SS ring for: a.) Model A with microstrip feed line similar to [15]; b.) Model B with microstrip feed line replaced by the coaxial feed line.

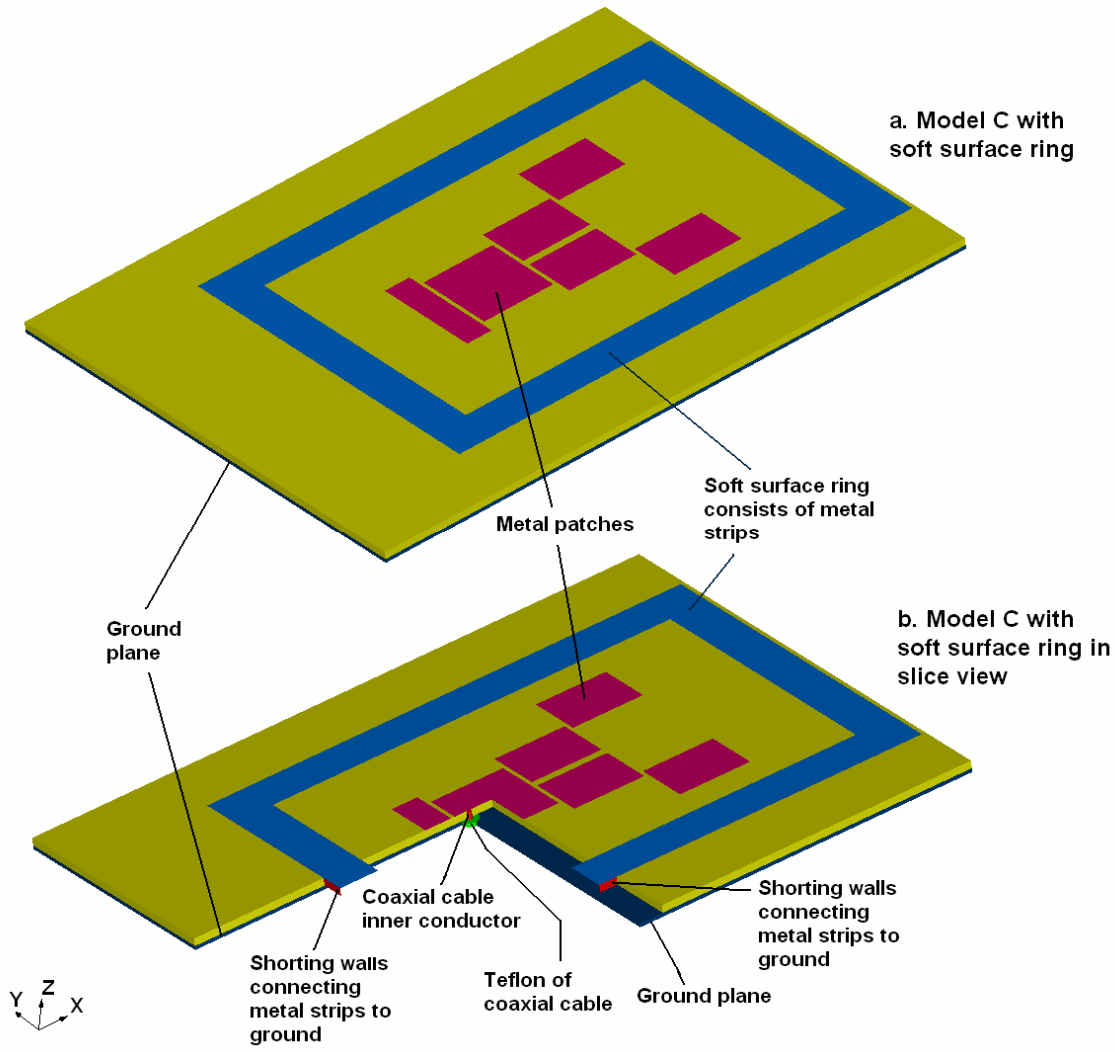

Figure 5. The topology of model C with SS ring on the same ground size with the design in [15] for a.) Model C in 3D view; and b.) Model C with slice view.

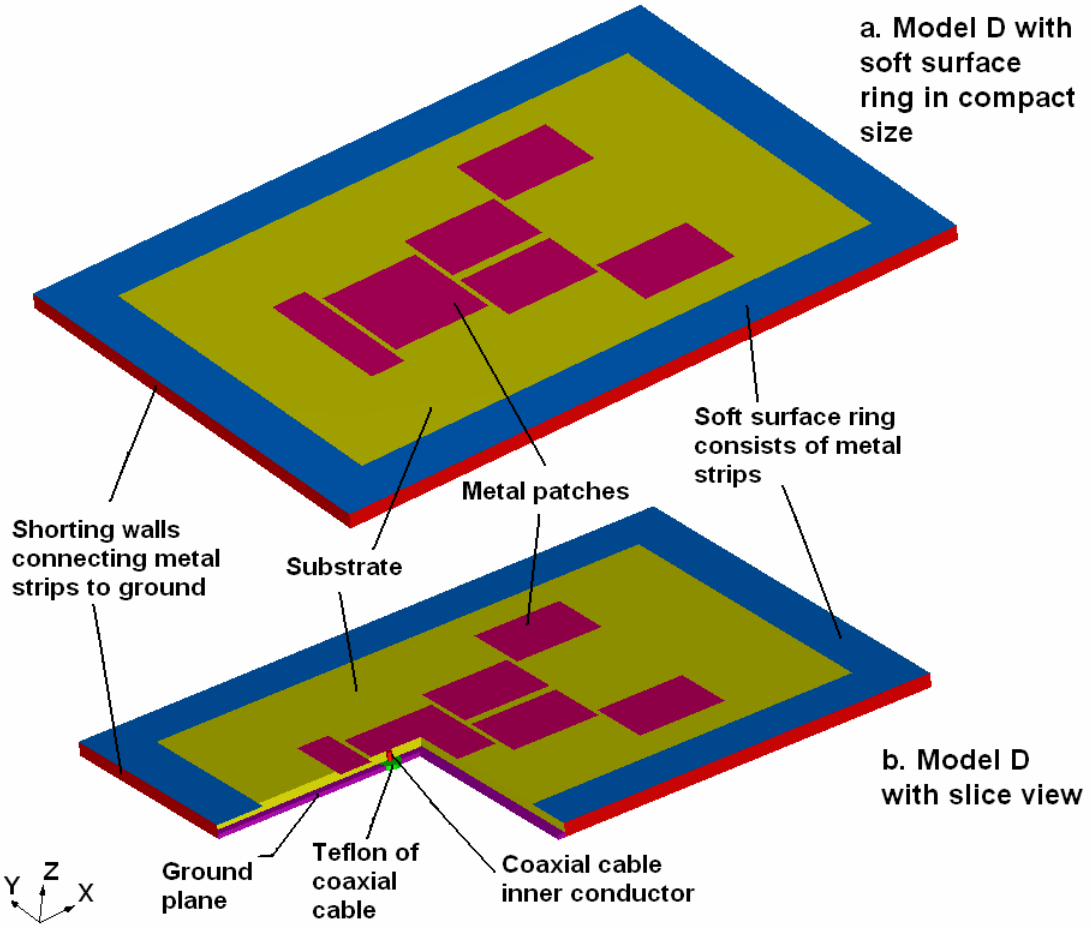

Figure 6. The topology of model D with SS ring in compact size for Model D a.) in 3D view; and b.) in slice view.

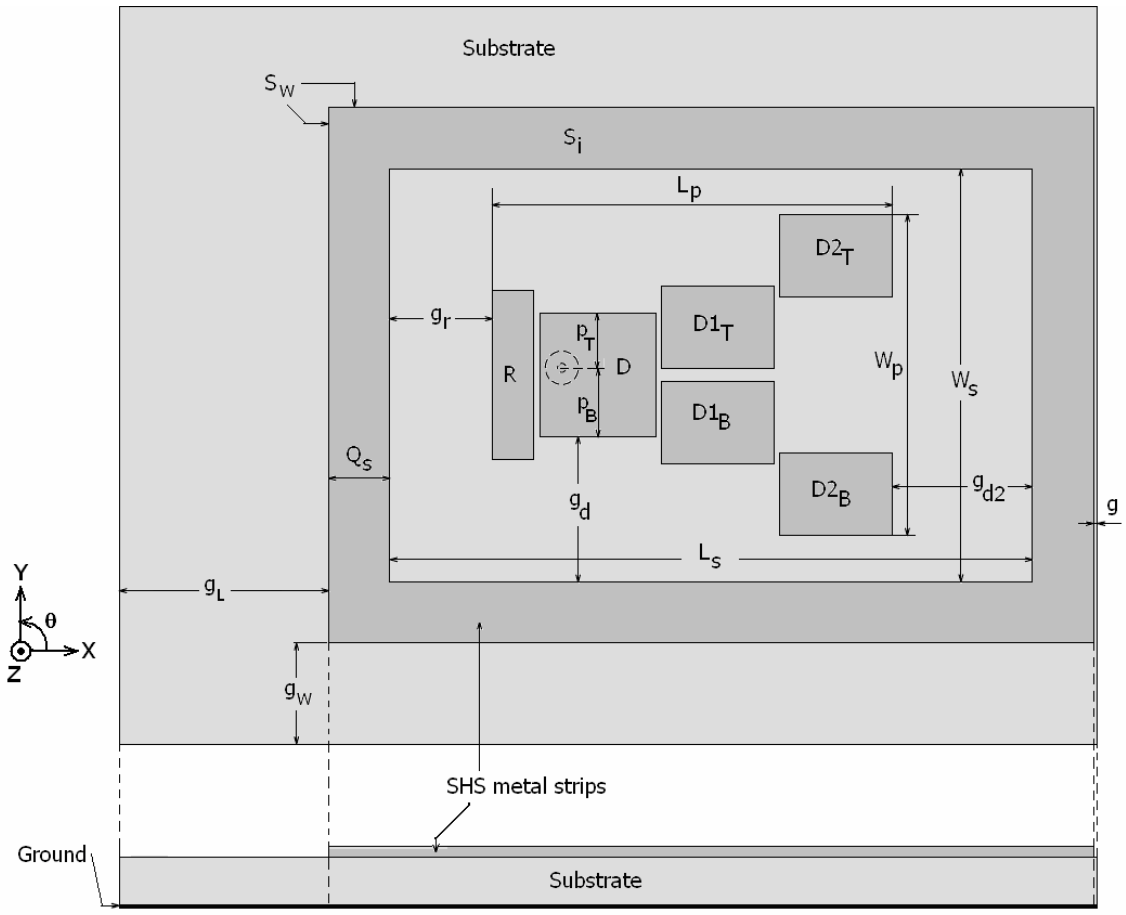

Figure 7. Two-dimensional view of model C with dimensional notations, model D can be envisioned by subtracting the ground and substrate outside the SS ring.

Table 1. SS Yagi array antenna physical dimensions in mils.

L_D	W_D	$L_{D1}=L_{D2}$	$W_{D1}=W_{D2}$	L_R	W_R	L_S	W_S
629	674	610	448	223	914	3484	2242
Q_s	p_B	p_T	g_r	g_d	g_{d2}	g_L	g_w
332	377	297	558	784	758	1132	549

IV. PRINCIPLES OF OPERATION

The mechanism for improvement in radiation characteristics of the antenna is achieved by two factors: 1) the first is the surface wave suppression achieved by the high impedance of the SS ring that blocks the power flow normal to its surface and 2) the second is the radiation of the SS ring constructively contributing to the radiation of the

antenna patches because of the coupling between the SS metal strips and the patches that further improve the F/B ratios.

In the first factor, as the surface waves flow outward from the source (the radiating patches) toward the edge of the substrate, they impinge upon the SS ring that consists of the quarter-wavelength strips shorted to ground on the outer edge serve as an open-circuit for the TM10 mode (the fundamental operating mode for a patch antenna). Therefore, the SS ring creates a high impedance boundary that blocks the surface current from flowing outward beyond the outer edge of the SS ring as illustrated in Fig. 8 [18]. The surface wave is then converted into a standing wave that is trapped inside the SS ring cavity (as shown in Fig. 10b) where the electric field distribution is captured inside the substrate (37 mils above the ground plane). Such a standing wave is not observed in Fig. 9b, where the electric field distribution on the E plane is captured in the air at 1 mil above the surface of the metal strips. As a result, the surface waves can be suppressed outside the SS ring thus alleviating the diffraction of the surface wave at the substrate edges; therefore the intended radiation pattern of the microstrip Yagi antenna is improved.

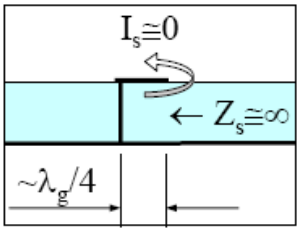

Figure 8. Illustration of SS operating principles. The current beyond the SS walls is close to zero due to high impedance of the quarter-wave SS strip shorted to ground.

The second factor is attributed to array coupling between the SS metal strips and the driven and director patches of the antenna. In particular, the two SS metal strips in the x-direction, together with the driven and the director D1 and D2 patches form a five-

element array, further improves the radiation in the quasi-endfire direction (quadrant I). Due to the constructive interference of the R-D-$D1_T$-$D2_T$ and the R-D-$D1_B$-$D2_B$ single microstrip Yagi arrays [15], the two directors, $D1_T$ and $D1_B$ patches are considered as a single effective array element with its effective aperture in the coupling five-element array, and the two directors, $D2_T$ and $D2_B$ patches, are considered as another single effective array element with its effective aperture. The effective aperture of the two single effective array elements is demonstrated by the surface current distribution shown in Fig. 9a. The operation of the five-element array is based on the coupling of the fringing field at the inner edge of the metal strip S1 (Fig. 9a) with the nearest radiating edge of the driven patch; and the coupling of the fringing field at the inner edge of the metal strip S3 (Fig. 9a) with the nearest radiating edge of the effective array element formed by director D2 patches. Even though the magnitude of the fringing field along the inner edges of the SS metal strips may be much lower than that of the antenna patches, the size of the ring is much larger than the patches so that the total fringing field along the metal strips (S1 and S3) exhibits constructive interference and becomes comparable to that of the patches. Thus the effective contribution to the operation of the five-element array (in the E plane) can be significant. This coupling effect can be observed directly from Fig. 9b where the electric field distribution is captured at the distance of 1 mil above the surface of the metal patches in the z direction to the radiation field is strongly active at the inner edges of the metal strips S1 and S3. No such coupling is observed in Fig. 10b where the electric field distribution is captured inside the substrate. In the topology of Fig. 7, the inner length of the SS ring, L_S becomes the factor that determines the separation between the metal strip S1 and the driven patch as well as the separation of the metal strip S3 and the

director D2 patches. Additionally, the inner width of the ring, W_S, becomes the factor that determines the size of the metal strips S1 and S3. Therefore, the optimized spacing (denoted g_{d2} as in Fig. 7) between the metal strip S3 and the director D2 patches is approximately 0.4 λ_o, while the optimized spacing (denoted g_r as in Fig. 7) between the metal strip S1 and the driven patch is approximately 0.3 λ_o. W_S is approximately one λ_o.

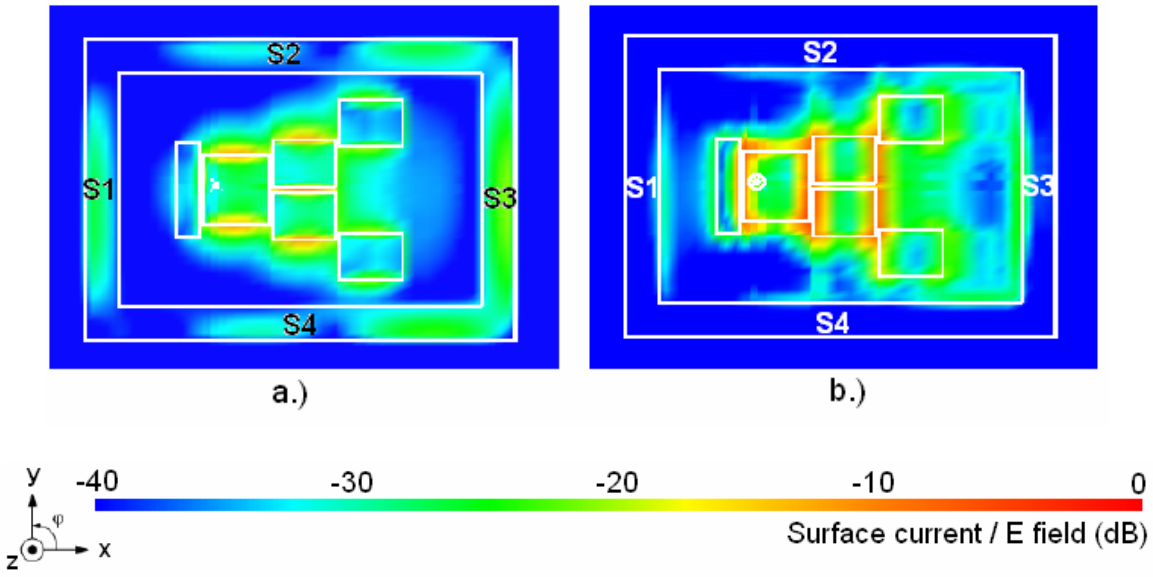

Figure 9. Peak magnitude distribution of the SS microstrip Yagi array antenna at 5.8 GHz of a.) the surface current; and b.) the electric field intensity in the x-y plane at 1 mil above the metal patches' surface (63 mils above the ground plane).

It is important to note that the SS ring not only functions as a high surface impedance structure that blocks the surface wave, but also acts as a resonant structure that constructively supports the radiation of the Yagi antenna. In contrast to conventional large-area artificial SS surfaces where the thickness of the slab determines the central operating frequency, the shorting of the metal strips in the modern SS structure provides conditions for high surface impedance, and the operating frequency is determined by the

strip width [17], not by the thickness of the substrate. As discussed earlier, the operating principles of the SS ring when applied to the microstrip Yagi antenna arrays explain how the radiation pattern can be improved not only for an arbitrary thickness of the substrate, but also for a significantly reduced ground size in terms of the size required for the best radiation performance in conventional patch antennas [20][21]. In the new configuration, the area of the ground plane that is beyond the SS ring has relatively no effect on the antenna's performance; hence, the ground size can be reduced without affecting the radiation performance of the SS microstrip Yagi array, and lead to the compact design shown in model D (Fig. 6).

V. SS PARAMETRIC ANALYSIS

The antenna is placed near the center of the ring due to the symmetry of the surface waves propagating outward as well as the symmetry of the SS ring in response to these surface waves. The location of the antenna is precisely in the middle of the dimension W_S, and is slightly off center with respect to dimension L_S. This asymmetry, where g_r is slightly smaller than g_{d2} (Fig. 7), is due to the fact that g_r is the distance from the reflector R, to the SS strip, while g_{d2} is the distance from the coupling patches, D2's to the SS strip. The reflector does not radiate equally strong with the patches D2's, however the driven, D next to the reflector radiates stronger than D2's. The asymmetry is due to the dependency of the distances on the combined effect of all of those factors.

There are three major parameters that affect the performance of the SS structure, and they are based on the two operational principles described earlier: the width of the metal strip (Q_S), the inner length of the SS ring (L_S), and the inner width of the SS ring

(W_S). A parametric analysis is performed to investigate the variations of these parameters above and below their optimized values while the optimized values of the remaining parameters are maintained. All the results discussed in this section are obtained through simulations using MicroStripes 7.0 by Flomerics, Ltd. (an electromagnetic simulation software package which solves for the fields via the transmission-line matrix (TLM) method). The lengths of each side of the ground plane are extended up to a factor of 1.5 in the simulations to maintain consistency in the analysis because it is well known that variations in the size of the ground plane can adversely affect the results [20],[21]. The variations of Q_S, L_S, and W_S in terms of physical and electrical length are listed in Table 2. The parameter Q_S is varied by an amount ΔQ_S above and below its optimized value of 0.25 λ_g, where λ_g is the guided wavelength. The parameter L_S and W_S are varied by ΔL_S and ΔW_S, respectively above and below their optimized values where ΔL_S and ΔW_S are chosen with respect to the free space wavelength, λ_o. To investigate the operational principles stated in section IV, different deviations are applied to different parameters because they are operating based on different principles. Since Q_S has a value around 0.25 λ_g upon which the open circuit factor is determined, its parametric investigation is centered upon this value to observe its effect on the performance of the high impedance surface. On the other hand, L_S and W_S are in the value ranges of about λ_o because these parameters determine the coupling fields in free space. Note that the variations in parameter Q_S are much smaller than those in parameters L_S and W_S.

Table 2. Deviations of Q_S, L_S, and W_S used in the parametric study.

ΔQ_S	Physical length	±20 mils	±60 mils	±100 mils
	Electrical length	±0.015 λ_g	±0.045 λ_g	±0.075 λ_g
ΔL_S	Physical length	±100 mils	±150 mils	±250 mils
	Electrical length	±0.05 λ_o	±0.12 λ_o	±0.25 λ_o
ΔW_S	Physical length	±60 mils	±100 mils	+150 mils
	Electrical length	±0.03 λ_o	±0.05 λ_o	+0.12 λ_o

a. Variation of metal strip width, Q_S

In this variation, L_S and W_S remain at their optimized values; and the width, Q_S, of the four metal strips is increased and decreased with the position of the inner edges of the strips being fixed. The field trapped by the SS ring with the width of $\lambda_g/4$ is shown in Fig. 10, where the planar cut of the captured field is inside the substrate at 37 mils above the ground plane in the z-direction.

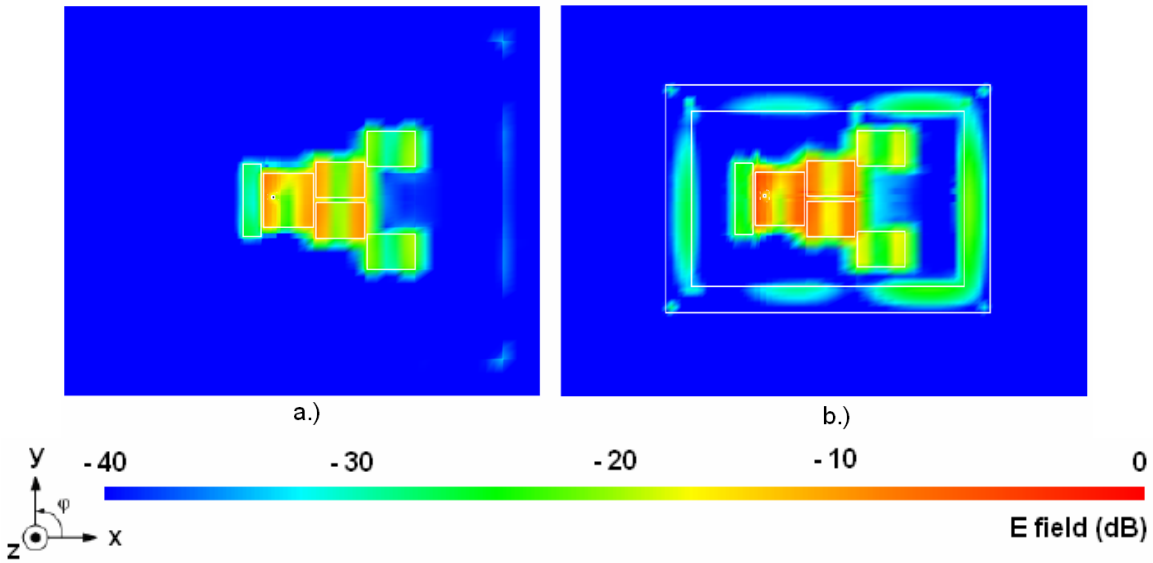

Figure 10. Electric field distribution inside the substrate at 37 mils above ground plane at 5.8 GHz for the SS printed microstripYagi array antenna for a.) Model B (no SS) and b.) Model C with the optimized Q_S.

The surface wave mode is observed to be trapped effectively within the SS ring when the metal strip width is $\lambda_g/4$. Because the fundamental mode of the surface wave is blocked by the open-circuit metal walls, it induces a resonance within the SS cavity as shown in Fig. 10b. It can be observed in Fig. 10a, where the SS structure does not exist, that the surface waves can freely propagate toward the edge of the substrate and ground plane, encounter these discontinuities, and result in the diffraction (in the x-direction) that is detrimental to the radiation pattern. The SS metal strips act as high surface impedance and stop the power flow of the surface waves in the direction perpendicular to the strips, while allowing its flow in a parallel direction. Thus, the SS ring as a whole acts as a waveguide that can hold this power of the surface waves locally (in the standing wave form) and also transform part of this power into useful radiation by the coupling field effect, the second operating principle discussed in section IV. The SS ring waveguide enhances the radiation pattern of the antenna. The SS waveguide has its aperture formed by the width of the metal strip and the thickness of the substrate, while the length of this waveguide is the effective perimeter of the rectangular SS ring (about the average of the outer and inner perimeters). For the SS model in Fig. 10b, the condition of $\lambda_g/4$ for the metal strip width allows the cavity to be optimized in accommodating the fundamental mode of the surface wave. As a result, when the strip width is decreased or increased (while holding L_S and W_S at their optimized values), both functions of the SS ring mentioned earlier are suppressed at various levels.

In the first case, as the strip width is decreased, the frequency at which the shorted metal strips behave as an open-circuit is shifted upward. Thus, the SS ring no longer forms an open-circuit with respect to the fundamental mode surface wave but rather

becomes an open-circuit to higher order modes. Therefore, it can be observed in Figs. 8a, 8b, 8c that the diffraction effects at the edge of the ground increase. In addition, the decrease in the strip width also results in smaller apertures; this shortens the lengths of the SS waveguides and lead to higher cut off frequencies. Hence, the resonance inside the SS ring gradually disappears as observed from Fig. 11 where the strip width is decreased by 0.015 λ_g, 0.045 λ_g, and 0.075 λ_g from the optimized value as shown in Figs. 8a, 8b, and 8c respectively. Therefore, the total effect that the shorten strip width causes is that fewer surface waves get trapped and less radiation enhancement occurs. Thus the SS ring becomes more transparent, and the electric field distribution looks closer to that of the non-SS model as shown in Fig. 10a.

In the second case, as the strip width is increased by 0.015 λ_g, 0.045 λ_g, and 0.075 λ_g from the optimized value, the open-circuited frequency of the metal strips is shifted downward, that is it becomes lower than the fundamental mode of the surface wave. Similar to the first case, this shifting of frequency away from the fundamental mode decreases the surface impedance of the SS ring, thus fewer surfaces are stopped from flowing toward the edge of the substrate and ground plane, and results in an increasing diffraction effect as observed in Fig. 11e, 8f, and 8g. However, different from the first case, the increase in the metal strip width results in bigger aperture and longer effective length of the SS waveguides which have lower cut off frequencies. Therefore the SS waveguide can hold as much power of the surface waves as is trapped by the open-circuit effect and transform a bigger portion of the trapped power into useful radiation. As a result, the models with increased strip width have slightly higher F/B ratios as indicated in Table 3 (where F/B-Right and F/B-Left ratios of different models

with various Q_S values are summarized). The F/B ratios in Table 3 are obtained with the ground size extended (in simulations) as mentioned earlier. Note that the waveguide effect of the SS ring can be observed clearly in Fig. 11e, 8f, and 8g. The frequency of the standing waves increases (more bright and dark regions) as the strip width shifts further from the optimized value; this increase in the number of bright and dark regions indicates that the surface waves being trapped within the SS ring waveguide are due to higher order modes because lower order modes (with more power) were not stopped from flowing outward by the shorted metal walls. This observation confirms the lower impedance surface factor discussed earlier and also the waveguide effects of the SS ring.

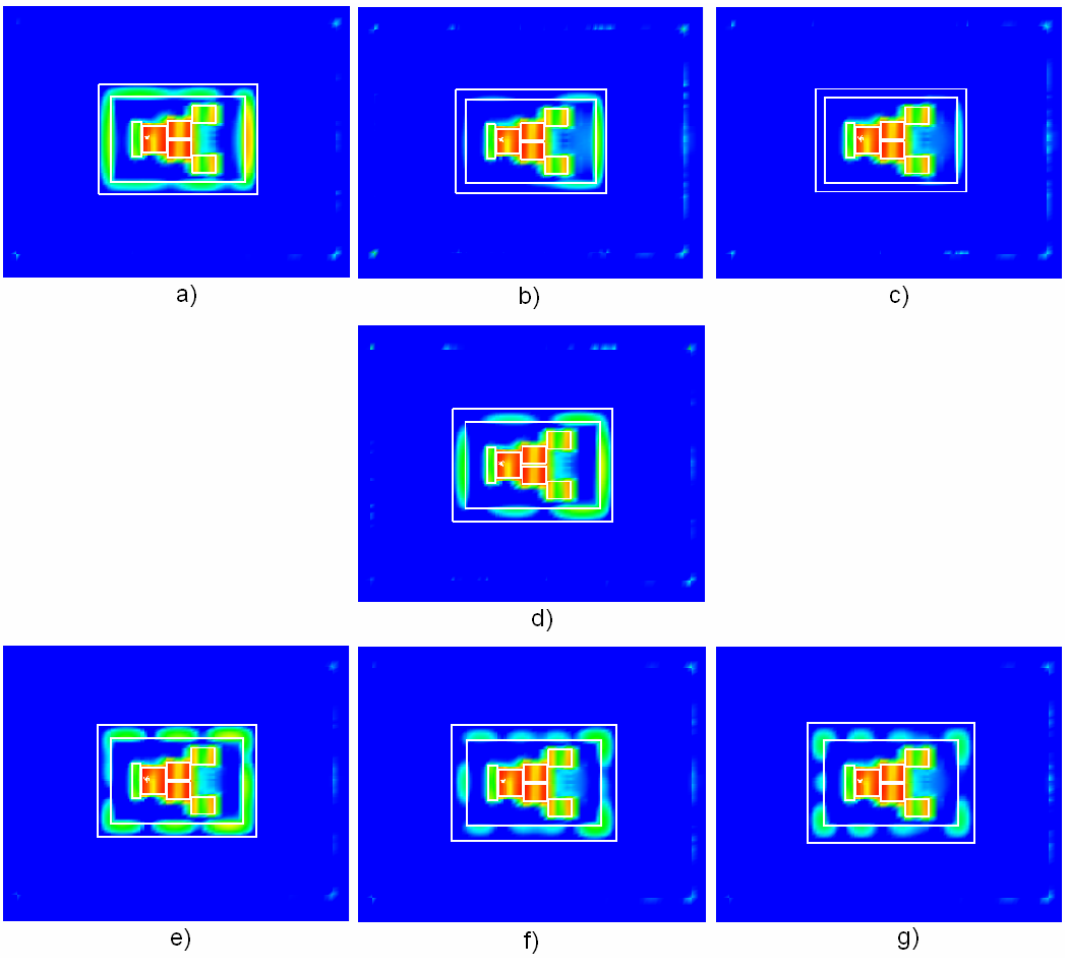

Figure 11. Electric field peak magnitude distribution at 5.8 GHz inside the substrate at 37 mils above the ground plane of different variation in Q_S for a.) ΔQ_S= -0.015 λ_g; b.) ΔQ_S= -0.045 λ_g ; c.) ΔQ_S= -0.075 λ_g; d.) ΔQ_S= 0; e.) ΔQ_S= +0.015 λ_g; f.) ΔQ_S= +0.045 λ_g; and g.) ΔQ_S= +0.075 λ_g.

Table 3. Comparison of F/B-Right and F/B-Left of models with variation in Q_S.

ΔQ_S	F/B-Left (dB)	F/B-Right (dB)
-0.075 λ	14.9	16.2
-0.045 λ	15.7	16.0
-0.015 λ	15.0	17.9
optimized	16.6	18.1
+0.015 λ	14.6	17.4
+0.045 λ	15.2	17.2
+0.075 λ	15.4	17.0

In Table 3, the values of F/B-Left and F/B-Right are not linearly increased or decreased in comparison to the optimized value. These variations are due to the F/B ratios being taken from the peak values in specific quadrants, but the lobes in a quadrant change more dynamically and have more than one local maxima as observed in quadrant II of $-90^o \leq \theta \leq 0^o$. Depending on the mode of the standing wave resonating within the SS waveguide, the E field intensity is distributed differently along the SS ring and affects the coupling field at the inner edges of the SS ring. For instance, the unusual high lobe at -30^o of curve (a) in Fig. 12 is attributed to the high intensity of the E field resonating under the metal strip S1. Fig. 12 shows the real part of co-polarization E field being plotted against angle θ on the E-plane cut (x-z plane) of the radiation patterns at 5.8 GHz for different Q_S values of the microstrip Yagi array antenna while having the SS ring implemented on the extended ground plane. In general, the width of the main beam

(whose peak is about 30°) is increased as $|\Delta Q_S|$ is increased.

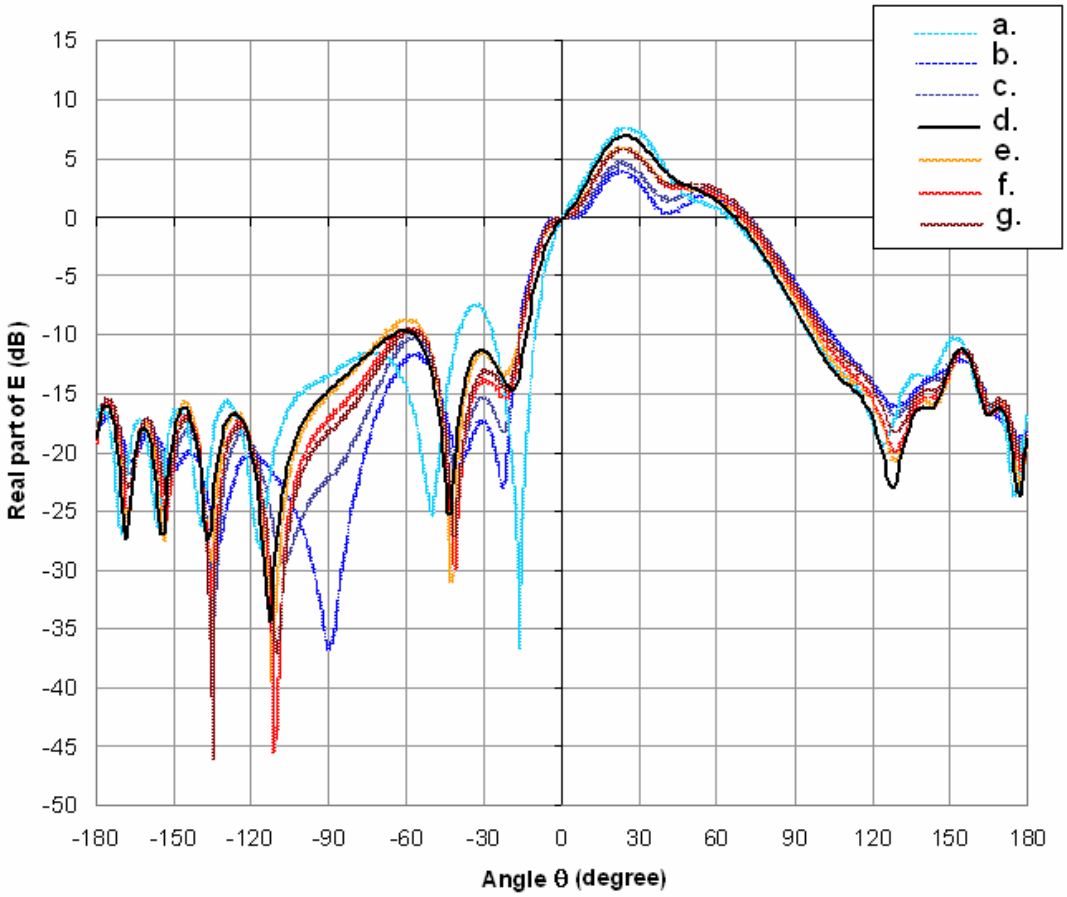

Figure 12. Real part of E field in co-polarization on E plane at 5.8 GHz of different variations in Q_S for
a.) ΔQ_S= -0.015 λ; b.) ΔQ_S= -0.045 λ; c.) ΔQ_S= -0.075 λ; d.) ΔQ_S= 0 λ;
e.) ΔQ_S= +0.015 λ; f.) ΔQ_S= +0.045 λ; and g.) ΔQ_S= +0.075 λ.

b. Variation of SS ring inner length, L_S

It was reported in section IV that the parameter L_S is the dominant factor over the coupling mechanism. Recall that the coupling mechanism is enabled by the forming of the five-element array that consists of the metal strips S1 and S3 (Fig. 9), the driven patch, the director 1 (D1) and director 2 (D2) patches. Therefore, the variations of L_S

around the optimized value depend on the parameters g_{d2} and g_r (Fig. 7) which strongly affect the coupling. A closer spacing results in higher directivities and higher F/B ratios because the increased spacing allows for stronger array coupling. Fig. 13 shows the electric field distribution at 1 mil above the surface of the metal patches in the z-direction when different variations applied to L_s are studied.

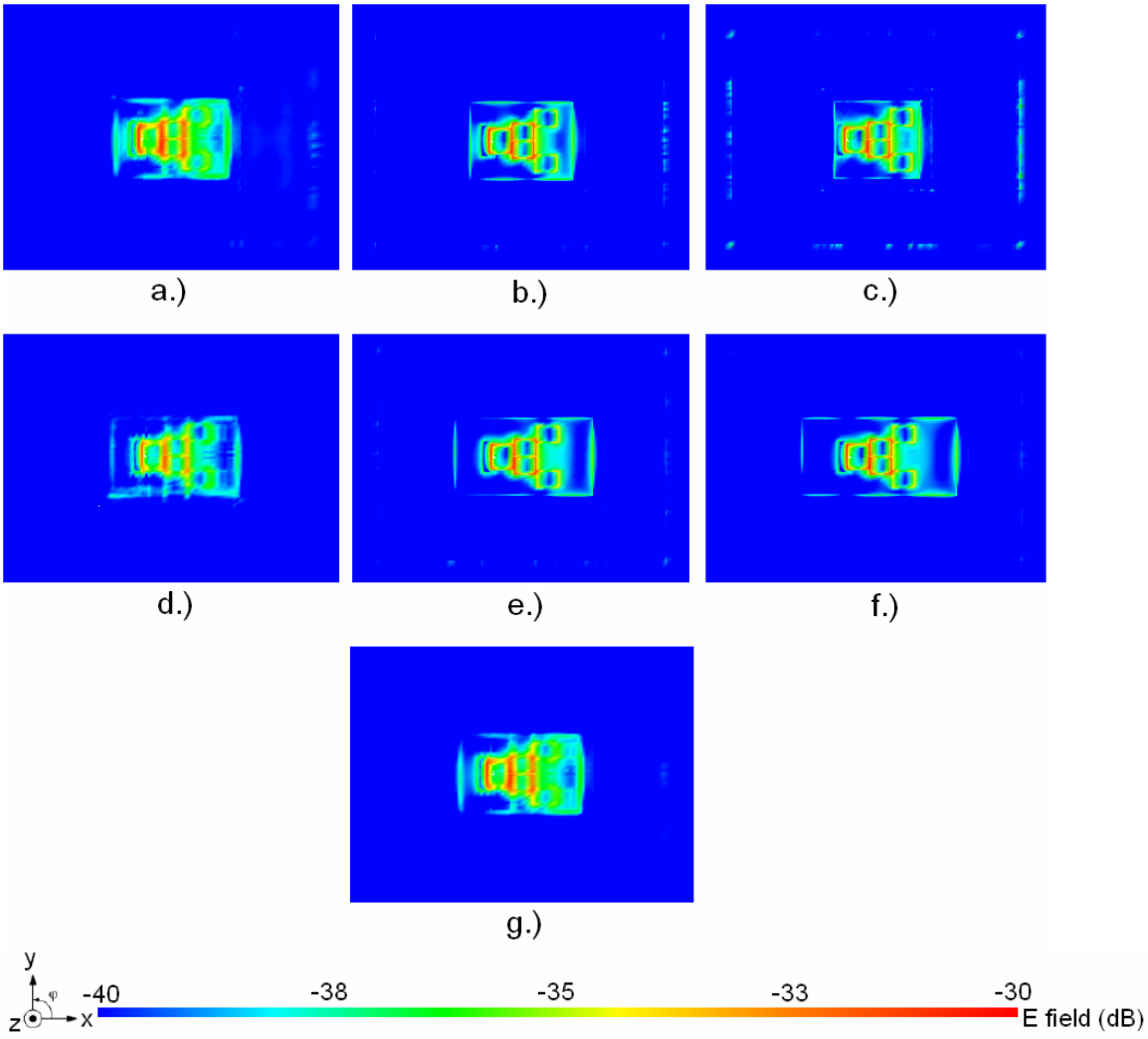

Figure 13. Peak magnitude distribution of the electric field at 1 mil above the metal patches (63 mils from ground plane) at 5.8 GHz for a.) ΔL_S= -0.05 λ_O; b.) ΔL_S= -0.12 λ_O; c.) ΔL_S= -0.25 λ_O; d.) ΔL_S= +0.05 λ_O; e.) ΔL_S= +0.12 λ_O; f.) ΔL_S= +0.25 λ_O; and g.) ΔL_S= 0 (optimized).

As L_S is decreased from the optimized value, both g_r and g_{d2} become smaller and the coupling of the fringing field is enhanced. However, the leakage of the surface wave is increased as observed in Figs. 10a, 10b, and 10c (in contrast to Fig. 13f where L_S is at its optimized value of about 1.7 λ_o). This leakage is due to the fact that the SS ring walls act as an open-circuit boundary that stops the flow of the surface wave while the SS ring itself acts as a cavity that effectively holds the surface wave energy locally. Therefore this energy does not interfere with the operation of the radiating patches that generate space waves. Therefore, as the SS ring cavity becomes smaller (where its cutoff frequency is higher than the surface wave mode), the diffraction effect becomes more significant at the edges of the substrate and ground plane as shown in Figs. 10b and 10c. As L_S is increased from its optimized value, the coupling field falls off quickly as shown in Figs. 10d, 10e, and 10f because the coupling effect is highly sensitive to the separation of the two coupled fields. If the radiating edge of the metal strip S3 or the radiating edge of the effective aperture of the D2 patches is considered as a finite dipole, then the magnitude of the electric field of this edge in the near field region decreases as the distance cubed (r^3). These effects are summarized in Table 3 where the directivities of different variations are shown to illustrate the principles described in this section.

c. Variation of SS ring inner length, W_S

As W_S is varied above and below the optimized value, there is only a small effect on the radiation pattern that can be observed. The directivity of the SS microstrip Yagi array antenna is about the same among the different variations of W_S as indicated in Table 4. The parameter W_S is limited by the geometry of the former microstrip Yagi

array antenna (design in [15]) such that it cannot be decreased further than approximately 0.05 λ_o on each side from its optimized value (W_S should not be less than W_p in Fig. 7, because the ring will overlap the patches). The size of the metal strips S1 and S3 are determined by W_S, and they give the best coupling effect when their inner edge lengths are approximately one λ_o long. The smallest size that S1 and S3 can be reduced to is roughly 0.9 λ_o which still allows the inner edge lengths of the metal strips to function well as coupling elements in the array. As W_S is increased above its optimized value, the edges of the metal strips S1 and S3 are increased beyond λ_o in length. Although increasing their sizes may enhance the fringing field for coupling, the coupling elements in an array have peak performance (low sidelobe levels) when their lengths are not longer than λ_o and their optimum spacing is about 0.5 λ_o. Therefore, as the length of S1 and S3 edges become larger than λ_o, the coupling of the fringing field in the five-element coupling array (in the x-direction) decreases, and causes a decrease (albeit by a small amount) in the directivity of the SS microstrip Yagi array antenna as indicated in Table 4. The little effects can be observed where the deviation from +0.03 λ_o to +0.12 λ_o is applied on W_S.

Table 4. Directivities at 5.8 GHz of the SS microstrip Yagi array antenna on extended ground size with different deviations in length of parameter L_S and W_S.

ΔL_S	-0.25 λ_o	-0.12 λ_o	-0.05 λ_o	0	+0.05 λ_o	+0.12 λ_o	+0.25 λ_o
Directivity	11.29 dBi	11.47 dBi	11.97 dBi	12 dBi	11.87 dBi	11.56 dBi	10.99 dBi
ΔW_S		-0.05 λ_o	-0.03 λ_o	0	+0.03 λ_o	+0.05 λ_o	+0.12 λ_o
Directivity		12 dBi	12 dBi	12 dBi	11.99 dBi	11.98 dBi	11.98 dBi

VI. SIMULATED AND MEASURED RESULTS

The simulated 2D cuts of co-polarized components in the E-plane of models A, B, C, and D are plotted in Fig. 14. The simulation results in Fig. 14 show that the F/B-Right ratio in the models with the SS ring is improved compared to the non-SS models by at least 3 dB, while a high F/B-Left ratio is maintained. Furthermore, the simulation results also show that the size of the microstrip Yagi array antenna can be reduced from 5300 x 4000 mils of model A to 4135 x 2904 mils of model D without compromising the performance. Notice that non-SS model (B) and SS model (C) have the same size with the same feeding method (coaxial line), but model C has the F/B-Right ratio improved by 3dB compared to that of model B, while maintaining the F/B-Left ratio reasonably close; the combined improved effect on these two F/B ratios in model C is indicated by a higher directivity. From the results in (C) and (D), it can be concluded that the change in feeding mechanism does not contribute to the improvement in F/B ratios observed in Fig. 14. This is a reduction by a factor of two in the total lateral size of the antenna. The F/B ratios and directivities from the simulations of the four models are summarized in Table 5 showing the improvement of the SS models C and D compared to the non-SS models A and B.

Table 5. Summary of F/B-Right, F/B-Left, and directivities of different models.

Model	Model A (no SS with microstrip feed line)	Model B (no SS with coaxial feed line)	Model C (SS on initial ground size)	Model D (Compact SS ring)
F/B-Right	16.0 dB	16.1 dB	19.2 dB	19.1 dB
F/B-Left	20.3 dB	17.2 dB	15.9 dB	18.3 dB
Directivity	11.0 dBi	10.38 dBi	11.6 dBi	11.6 dBi

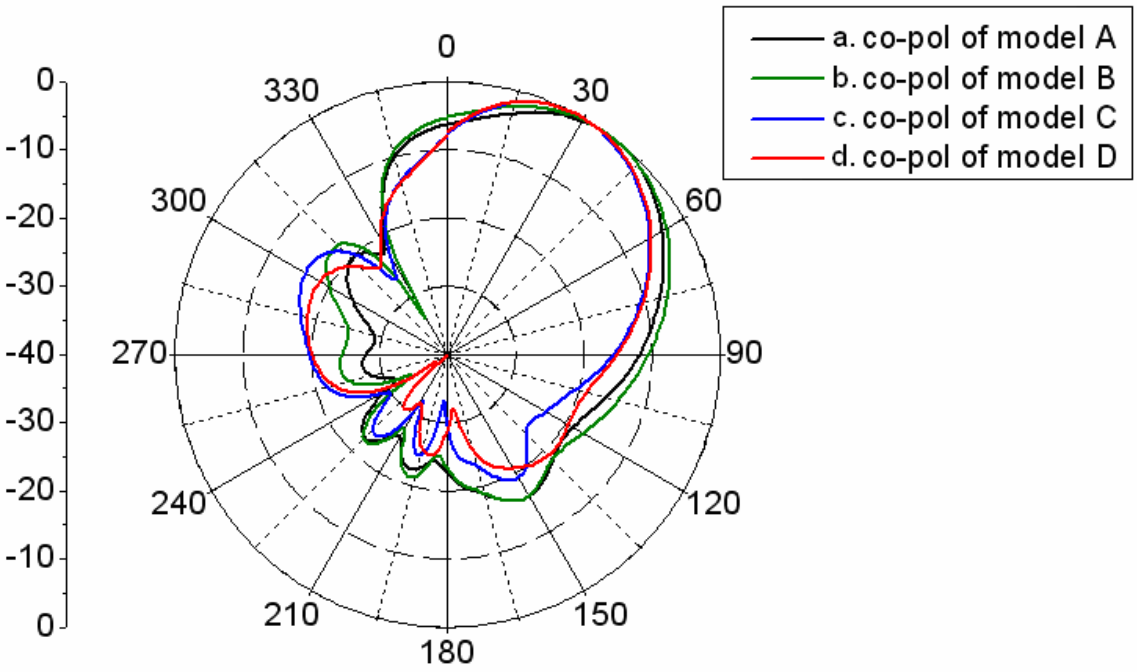

Figure 14. Co-polar plots on E-plane at 5.8 GHz of Microstrip Yagi array antenna for a.) Model A (no SS with microstrip feed line from [15]); b.) Model B (no SS with coaxial feed line); c.) Model C (with SS in big ground); and d.) Model D (with SS in compact size).

Model D was fabricated on a double copper (Cu) clad board of RT/duroid 5880 material (ε_r= 2.2) with a substrate thickness of 62 mils. The metal walls that short the metal strips of the SS ring to the ground are replaced by two rows of metal vias, with diameter and center-center separation equal to 10 mils and 20 mils, respectively. The vias have a diameter of 10 mils, and their separation is also 10 mils. The prototype of model D is shown in Fig. 15. Model A was also fabricated for comparison purposes. The measured results for the 2D cuts of the co-polarized and cross-polarized component in the E-plane of model D and model A are plotted in Fig. 16. The measured F/B-Left and F/B-Right ratios of the model D sample were recorded to be 20 dB and 22 dB respectively. The measurements were performed using the antenna measurement system Stargate 64 of Satimo, Inc. [22], where the first probe and the last probe leave a blind angle of about

60^o corresponding to the shaded region in Fig. 16 ($150^o \leq \theta \leq 210^o$). In measurement, the coaxial connector can act like a reflector that interferes with radiation in the regions close to it (see Fig. 15b), this interference contributes to the difference between measured and simulated data in the region of $135^o \leq \theta \leq 225^o$ shown in Fig. 16. Since the radiation immediate to the right of the coaxial connector (Fig. 15b) is expected to have stronger radiation than that to the left of the connector, the effect of the connector on the radiation in the region of $130^o \leq \theta \leq 230^o$ is stronger such that the beam may be steered upward (in +z direction) and results in a lower peak compared to simulated results. The measured F/B-Left ratio of the model D sample is about 5 dB higher than that of the model A sample (represented by the dash green curve in Fig. 16). This ratio is the ratio of the peak at 330^o of the dash green curve (model A prototype) to the peak at around 290^o of the blue curve (model D prototype) as shown in Fig. 16. Notice that the peak at 330^o of non-SS model A has been reduced significantly in SS model D.

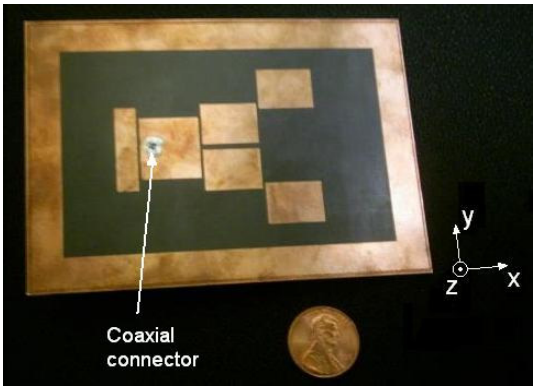

Figure 15a. The front view of the Soft-surface microstrip Yagi array antenna prototype showing the physical size of the antenna.

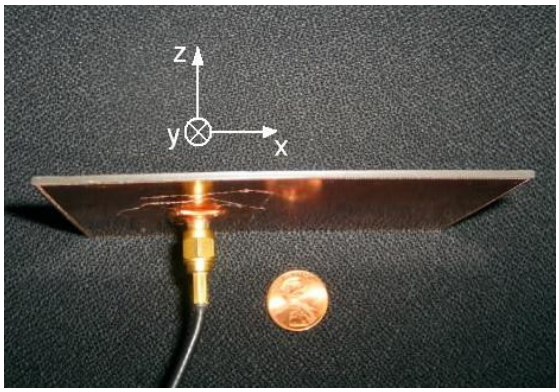

Figure 15b. The backside view of the Soft-surface microstrip Yagi array antenna prototype showing the coaxial connection.

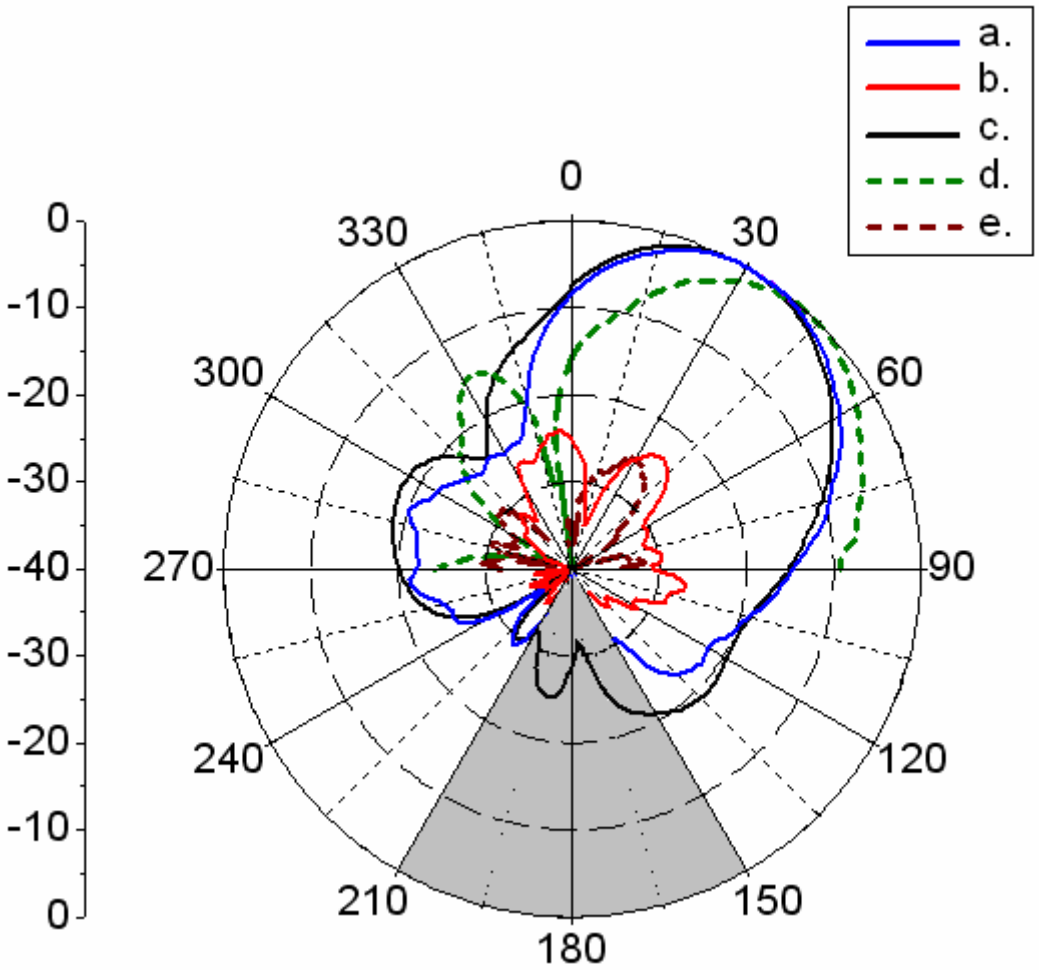

Figure 16. Radiation pattern on E-plane for model D sample at 5.8 GHz and model A sample at 5.2 GHz for
a.) Model D measured results of co-polarization in the range of $-180^{o} \leq \theta \leq 180^{o}$;
b.) Model D measured results of cross-polarization in the range $-180^{o} \leq \theta \leq 180^{o}$;

c.) Model D simulated results of co-polarization in the range $-180^{o} \leq \theta \leq 180^{o}$;
d.) Model A measured results of co-polarization in the range $-90^{o} \leq \theta \leq 90^{o}$;
e.) Model A measured results of cross-polarization in the range $-90^{o} \leq \theta \leq 90^{o}$.

The cross polarization from the model D sample (represented by the red line in Fig. 16) remains low, however, is generally higher than that observed in the model A sample (dash brown line in Fig. 16). The increase in the cross-polarization is due to the change in the feeding technique where the microstrip feed line in model A is replaced by the coaxial feed line in model D. In order to obtain the matching, the coaxial line is positioned off the center (in the y-direction) of the driven patch as shown in Fig. 7, and introduce an asymmetry in the feed that generates higher order modes, which contribute to the cross-polarized radiation.

The return loss of models A, B, C and D obtained from simulations and the return loss of the model D sample obtained from measurements are shown in Fig. 17. The impedance bandwidth is taken at the level of -10 dB, and is observed through simulation that the impedance bandwidth of the SS models (model C and D in red and black solid lines respectively) is similar to that of the non-SS model (model B in blue solid lines) (Here, only the coaxially fed models are compared.) In general, the SS models are subjected to a decrease in the impedance bandwidth due to the fact that the SS ring is a highly frequency dependent structure (the optimized metal strip width, Q_S, is $\lambda_g/4$). At frequencies off the resonant, the SS ring cannot trap surface waves as effectively as it can at resonant frequencies; thus, the quality (Q) factor due to space wave losses is increased. It is important to note that the impedance bandwidth of the antenna is limited by the SS bandwidth, but the degree of limitation is determined by the performance specifications of the design and its application. It can be easily observed in Fig. 17 that the simulated

impedance bandwidth of about 12 % of model A implemented with a microstrip feeding line (green solid line in Fig. 17) is bigger than the simulated impedance bandwidth of about 10 % of model B, C, and D implemented with a coaxial feeding line. As a result, despite the SS ring limitation explained earlier, the resulting impedance bandwidths of the SS models (model C and D) and the non-SS model (model B) in simulations are almost identical because the SS ring is also a radiating structure, which is the factor that compensates for the decrease in the impedance bandwidth caused by the limited bandwidth of the SS ring. However, the difference in the impedance bandwidth between model A (with a microstrip feeding line) and other models (with coaxial feeding lines) is potentially caused by the probe inductance introduced in the other models (model B, C and D) and results in an increase in their Q factors.

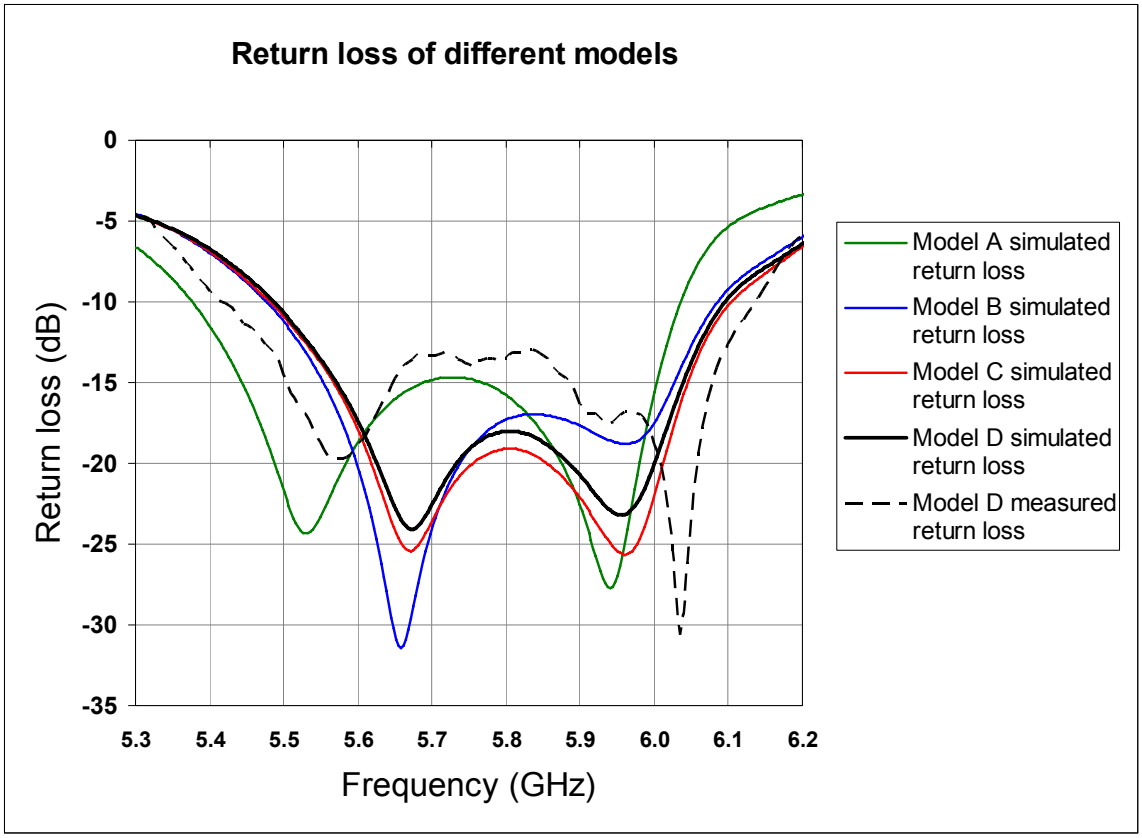

Figure 17. Frequency response of the simulated and measured results (S11-Parameter) of different models with center frequency of 5.8 GHz.

The directivities of models A, B, C, and D were plotted in Fig. 18. The directivity bandwidth is defined to be at the 10 dBi level. The SS models (model C and D) have directivity bandwidths around 14 %, while the non-SS models (model A and B) have the directivity bandwidths around 7 %. This ratio represents an improvement by a factor of two and shows the effectiveness of the SS ring.

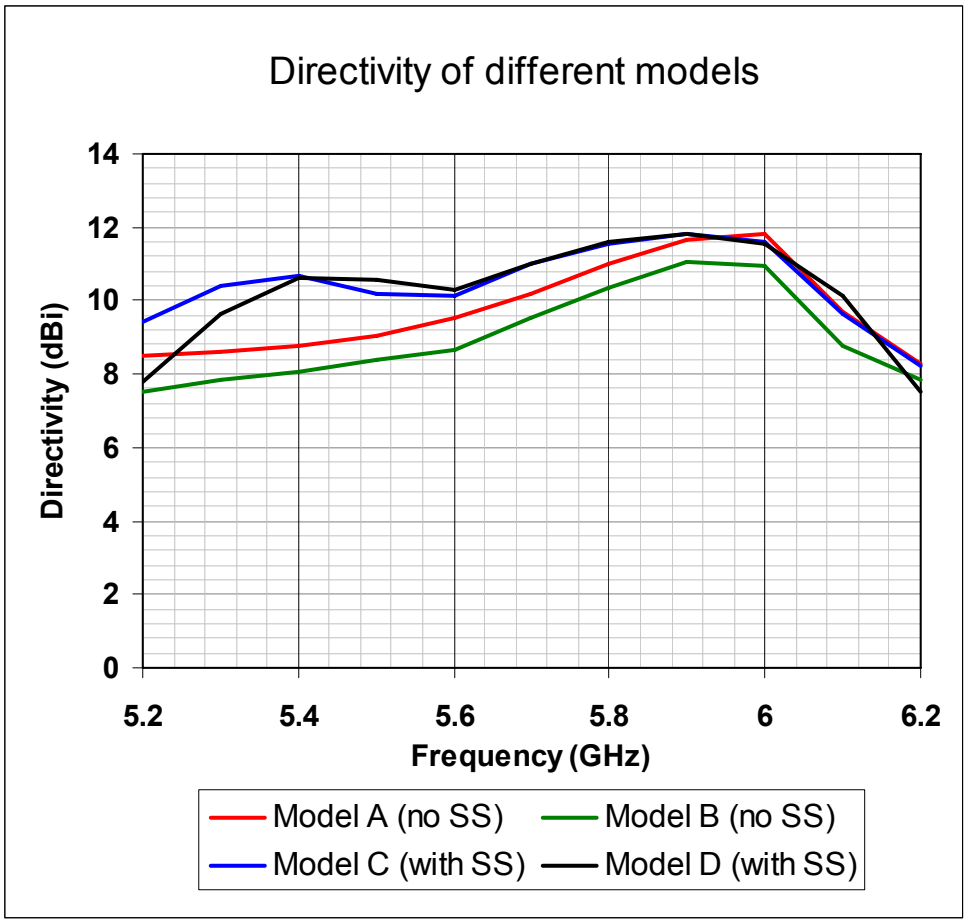

Figure 18. Directivities of model A, B, C, and D from simulations.

VII. CONCLUSIONS

A new antenna structure based on surrounding a microstrip Yagi array antenna with an SS ring is demonstrated to exhibit highly directional radiation in which the F/B ratios are improved to more than 20 dB; this value is approximately more than 3 dB higher than the conventional design without the ring. In addition, a high gain is maintained while the size of the structure is reduced by a factor of two. The operational principles of the SS ring have been analyzed via parametric studies of the critical dimensions of the design and justified through measurements. Vias are used in fabrication to realize the shorting walls of the SS structure in a low-loss configuration. The 10 dBi directional bandwidth in the SS models is twice as large as that of the non-SS models. This improvement enables an almost constant directivity over a large bandwidth, and allows applications such as wireless multimedia/HDTV devices to have more channels of signals without interference or degradation in signal quality. The application of the SS technique shown in this work is a robust method that can be implemented on generic planar structures to suppress unwanted radiation, improve the directivity and the F/B ratios, and reduce the total size of the antenna design.

REFERENCES

[1] C. A. Balanis, *Antenna Theory: Analysis and Design*, 2nd ed. New York: Wiley, 1997.

[2] R.E.Munson, "Conformal Micrsotrip Antennas and Microstrip Phased Arrays," IEEE Trans. Antennas Propag., vol. 22, no. 1, pp. 74-78, January 1974.

[3] K. R. Carver, J. W. Mink, "Microstrip Antenna Technology," IEEE Trans. Antennas Propag., vol. 29, no. 1, pp 2-24, January 1981.

[4] D. M. Pozar, "Microstrip Antennas," Proc. IEEE, vol. 80, No. 1, pp. 79-81, January 1992.

[5] [Online]. Available at http://www.manufacturers.com.tw/telecom/Yagi-Antenna.html, Oct. 2007.

[6] [Online]. Available at http://www.starantenna.com, Oct. 2007.

[7] J. Huang, "Planar microstrip Yagi array antenna," Procs. IEEE Antennas Propag. Society Int. Symp., Jun. 1989, vol. 2, pp. 894-897.

[8] A. Densmore and J. Huang, "Microstrip Yagi antenna for mobile satellite service," Procs. IEEE Antennas Propag. Society Int. Symp., Jun. 1991, vol. 2, pp. 616-619.

[9] J. Huang and A. Densmore, "Microstrip Yagi antenna for mobile satellite vehicle application," IEEE Trans. Antennas Propag., vol. 39, no. 7, pp. 1024-1030, July 1991.

[10] S. Padhi and M. Bialkowski, "Investigations of an aperture coupled microstrip Yagi antenna using PBG structure," Procs. IEEE Antennas Propag. Society Int. Symp., Jun. 2002, vol. 3, pp. 752-755.

[11] P.R. Grajek, B. Schoenlinner, and G. M. Rebeiz, "A 24 GHz high-gain Yagi-Uda antenna array," IEEE Trans. Antennas Propag., vol. 46, no. 5, pp. 605-608, May 1998.

[12] S. Ke and K. Wong, "Rigorous analysis of rectangular microstrip antennas with parasitic patches," Procs. IEEE Antennas Propag. Society Int. Symp., Jun. 1995, vol. 2, pp. 968-971.

[13] D. Gray, J. Lu, and D. Thiel, "Electrically steerable Yagi-Uda microstrip patch antenna array," IEEE Trans. Antennas Propag., vol. 46, no. 5, pp. 605-608, May 1998.

[14] D. Sievenpiper, L. Zhang, R.F.J. Broas, N.G. Alexopolous, and E. Yablonovitch, "High-impedance electromagnetic surfaces with forbidden frequency band," IEEE Transactions on Microwave Theory and Techniques, vol.47, no.11, pp. 2059-2074, November 1999.

[15] G. R. DeJean, M. M. Tentzeris, "A New High-Gain Microstrip Yagi Array Antenna With a High Front-to-Back (F/B) Ratio for WLAN and Millimeter-Wave Applications," IEEE Trans. Antennas Propag., vol. 55, no. 2, pp. 298-304, February 2007.

[16] R. L. Li, G. DeJean, M. Tentzeris, J. Laskar, and J. Papapolymerou, "LTCC multilayer based CP patch antenna surrounded by a soft-and-hard surface for GPS

applications," Proc. IEEE Antenna and Propagation Society International Symposium, Jun. 2003, vol. 2, pp. 651-654.

[17] G. Ruvio, P.-S. Kildal, and S. Maci, "Modal propagation in ideal soft and hard waveguides," Proc. IEEE Antenna and Propagation Society International Symposium, Jun. 2003, vol. 4, pp. 438-441.

[18] R.L.Li, G.DeJean, J.Papapolymerou, J.Laskar and M.M.Tentzeris, "FDTD Analysis of Microstrip Patch Antennas and Arrays on High Dielectric-Constant Substrate Surrounded by a Soft-and-Hard Surface", IEEE Trans. Magnetics, vol.40, no.2, pp.1444-1447, March 2004.

[19] P.-S. Kildal, "Artificially Soft and Hard Surfaces in Electromagnetics," IEEE Trans. Antennas Propag., vol.38, no.10, pp.1537-1544, October 1990.

[20] A. K. Bhattacharyya, "Effects of Ground Plane and Dielectric Truncation on the Efficiency of a Printed Structure," IEEE Trans. Antennas Propag., vol. 39, no. 3, pp. 303-308, March 1991.

[21] S. Noghanian, L. Shafai, "Control of Microstrip Antenna Radiation Characteristics by Ground Plane Size and Shape," IEE Proc. Microw. Antennas Propag., vol. 145, no. 3, pp. 207-212, June 1998.

[22] [Online]. Available at http://www.satimo.com, Oct. 2007.